Synthetic Approach for Tunable, Size-Selective Formation of Monodisperse, Diphosphine-Protected Gold Nanoclusters

ARTICLE *in* JOURNAL OF PHYSICAL CHEMISTRY LETTERS · SEPTEMBER 2010

Impact Factor: 7.46 · DOI: 10.1021/jz1009339

2 AUTHORS:

John Pettibone
National Institute of Standards and Technol…
28 PUBLICATIONS **769** CITATIONS
SEE PROFILE

Jeffrey W Hudgens
National Institute of Standards and Technol…
135 PUBLICATIONS **2,251** CITATIONS
SEE PROFILE

THE JOURNAL OF PHYSICAL CHEMISTRY Letters

pubs.acs.org/JPCL

Synthetic Approach for Tunable, Size-Selective Formation of Monodisperse, Diphosphine-Protected Gold Nanoclusters

John M. Pettibone[†] and Jeffrey W. Hudgens*

Chemical and Biochemical Reference Data Division, National Institute of Standards and Technology, Gaithersburg, Maryland 20899

ABSTRACT We report a new strategy that provides stringent control for the size and dispersity of ultrasmall nanoclusters through preparation of gold complex distributions formed from the precursor, $AuClPPh_3$ (PPh_3 = triphenylphosphine), and the L^6 (L^6 = 1,6-bis(diphenylphosphino) hexane) ligand prior to reduction with $NaBH_4$ in 1:1 methanol/chloroform solutions. Monodisperse nanoclusters of distinct nuclearity are obtained for specific ligand ratios; $[L^6]/[PPh_3]$ = 4 yields $[Au_8L^6{}_4]^{2+}$, $[L^6]/[PPh_3]$ = 0.4 yields $[Au_9L^6{}_4Cl]^{2+}$, and $[L^6]/[PPh_3]$ = 8 yields ligated Au_{10} cores in the form of $[Au_{10}L^6{}_4]^{2+}$ and $[Au_{10}L^6{}_5]^{2+}$. Polyhedral skeletal electron pair theory accounts for the stability of $[Au_9L^6{}_4Cl]^{2+}$, which is the smallest closed-shell chlorinated cluster reported. Electrospray mass spectrometry and UV−vis spectra indicate that $[Au_9L^6{}_4Cl]^{2+}$ and $[Au_{10}L^6{}_x]^{2+}$ (x = 4, 5) result from reactions involving $[Au_8L^6{}_4]^{2+}$. Syntheses of small gold clusters containing chloride ligands open the possibility of constructing larger clusters via ligand exchange.

SECTION Nanoparticles and Nanostructures

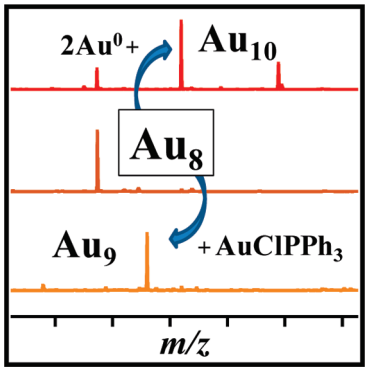

Synthetic methods for the production of phosphine-protected Au clusters have been the topic of extensive research for the last 30 years, with a significant portion devoted to nanoclusters capped by triphenylphosphine (PPh_3) ligands.[1−4] Solution-phase properties of gold nanoparticles are conveniently tuned by exchanging the phosphine cap with ligands possessing desired properties.[5−7] In contrast, aimed syntheses of monodisperse closed-shell clusters of chosen core nuclearity remain difficult and subject to the luck and skill of the experimentalist.[7] Some improvements of nanoparticle dispersity are obtained by controlling growth rates through adjustments of physical parameters (e.g., solvent, temperature, reductant strength, and stir rate). More recently, diphosphine ligands have shown promise for facilitating the formation of monodisperse gold clusters.[8−10] Bertino et al.[10] found that the mean gold core nuclearity obtained from synthesis solutions containing L^n diphosphine ligands changes with the length of the carbon chain, n, in the 1,n-bis(diphenylphosphino)n-alkane ligand. Thus, metal core size selectivity appears to be an inherent property of these bidentate ligands. Since solution metal complex equilibria are affected by the molar ratios among ligands, we hypothesized that cluster nuclearity and dispersity might be tunable through manipulation of the solution complex distribution. The present study shows that this strategy works for the case of L^6 and Au^I phosphine complexes. By controlling the complex distribution in solution, the synthetic products are able to be tuned, forming nearly monodisperse ligand-capped Au_8, Au_9, or Au_{10} clusters. This study also describes the preparation of the novel $[Au_9L^6{}_4Cl]^{2+}$, which is the smallest known, closed-shell, chlorinated cluster.

Using an electrospray ionization mass spectrometer (ESI-MS), we have measured the cationic reaction products volatilized from 1:1 methanol/chloroform solutions. Prior to addition of a reducing agent, sets of reaction vials containing $AuClPPh_3$ were also loaded with increasing amounts of L^6. The ligand content in each vial is described by $[L^6]/[PPh_3]$, where L^6 is the free and complexed L^6 ligands in solution, $AuClPPh_3$ is the only source of PPh_3, and $[PPh_3]$ is the total concentration of free and complexed PPh_3 ligands in solution. Reduction of the solutions generally yields the cationic products $[Au_8L^6{}_4]^{2+}$ and $[Au_9L^6{}_4Cl]^{2+}$ and the Au_{10} species, $[Au_{10}L^6{}_4]^{2+}$ and $[Au_{10}L^6{}_5]^{2+}$. These clusters display distinct UV−vis spectra and simple ESI mass spectra (Figure S1, Supporting Information) comprising their molecular ion peaks, which exhibit no evidence for ion fragmentation or neutral loss as the in-source ESI cone voltage is increased from +50 to +250 V. Such stability is consistent with the closed skeletal valence shells of these species.[11−15] Figure 1 shows the fractional product distribution among the cationic reaction products $[Au_8L^6{}_4]^{2+}$ and $[Au_9L^6{}_4Cl]^{2+}$, and the sum of $[Au_{10}L^6{}_x]^{2+}$ (x = 4 and 5) as a function of the ligand ratio $[L^6]/[PPh_3]$. The graph readily shows that nearly monodisperse nanoclusters

Received Date: July 9, 2010
Accepted Date: July 30, 2010
Published on Web Date: August 10, 2010

DOI: 10.1021/jz1009339 | J. Phys. Chem. Lett. 2010, 1, 2536–2540

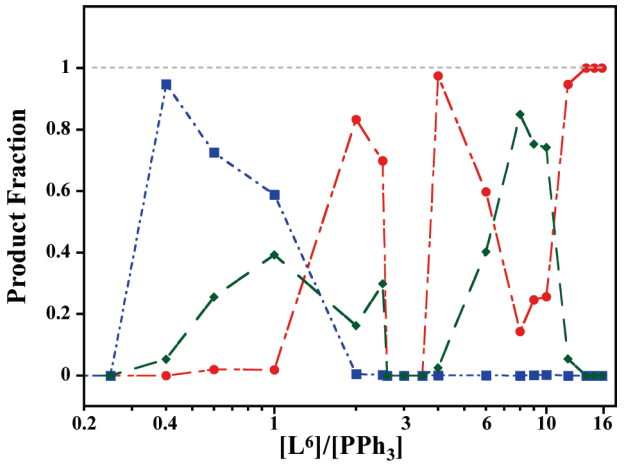

Figure 1. Fractional product distribution as a function of $[L^6]/[PPh_3]$. The symbols are assigned as follows: red circles, $[Au_8L^6{}_4]^{2+}$; blue squares, $[Au_9L^6{}_4Cl]^{2+}$; and green diamonds, $[Au_{10}L^6{}_x]^{2+}$ (x = 4 and 5). The product distribution was determined from fractional ion intensities measured with ESI-MS. See text for more details.

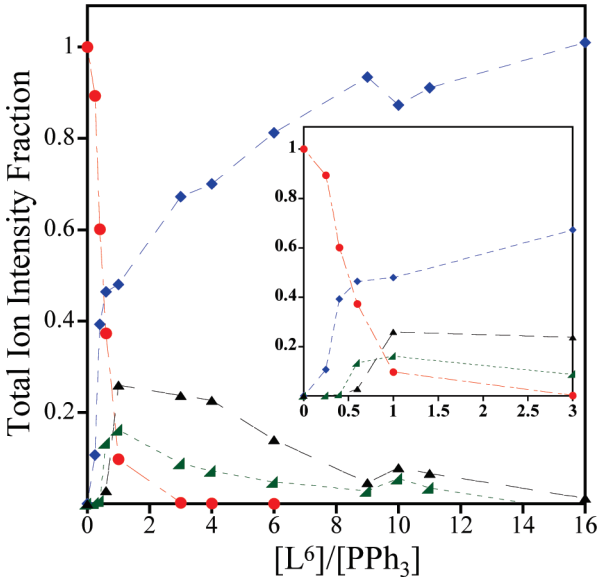

Figure 2. Fractional total ion current measured via ESI-MS as a function of the ratio $[L^6]/[PPh_3]$, where all PPh_3 originates from the chlorinated gold precursor, $AuClPPh_3$. As L^6 is added incrementally to a solution comprising 10.0 mg of $AuClPPh_3$ dissolved in 1:1 $CH_3OH/CHCl_3$, PPh_3 ligands are increasingly replaced on the metal complexes. The symbols are assigned as follows: red circles, $[Au(PPh_3)_2]^+$; blue diamonds, $[Au_2L^6{}_2]^{2+}$; green wedges, $[Au_2L^6{}_2Cl]^+$; and black triangles, $[Au_2L^6{}_3Cl]^+$. The inset displays the fractional total ion current for $0 \le [L^6]/[PPh_3] \le 3$.

of distinct nuclearity are obtained for reaction mixtures containing specific ligand ratios; $[L^6]/[PPh_3]$ = 0.4 yields $[Au_9L^6{}_4Cl]^{2+}$, $[L^6]/[PPh_3]$ = 4 yields $[Au_8L^6{}_4]^{2+}$, and $[L^6]/[PPh_3]$ = 8 yields $[Au_{10}L^6{}_x]^{2+}$ (x = 4 and 5).

The ligand−metal complex distribution as a function of $[L^6]/[PPh_3]$ is measured at equilibrium by observing the constant fractional ion intensities of the complexes prior to reduction (Figure 2). For $[L^6]/[PPh_3] \approx 0.25$, $[Au(PPh_3)_2]^+$ is the dominant solution complex, and only traces of $[Au_2L^6{}_2]^{2+}$, $[Au_2L^6{}_2Cl]^{2+}$, and $[Au_2L^6{}_3Cl]^{2+}$ are observed; hence, during reduction, the synthesis chemistry of $[Au(PPh_3)_2]^+$ (and $AuClPPh_3$) dominates, and the final products are similar to those obtained without the presence of L^6. As L^6 is added, the $[Au(PPh_3)_2]^+$ diminishes until $[L^6]/[PPh_3] \ge 3$, where its signal falls below the ESI-MS detection limit. (Note, L^3 and L^5 complexes combine with gold, forming $[Au(PPh_3)_xL^n{}_{2-x}]^+$ complexes,[16] whereas, the analogous Au:L^6 complexes are not observed.) Further, addition of L^6 causes the fractional abundances of $[Au_2L^6{}_2Cl]^+$ and $[Au_2L^6{}_3Cl]^+$ to increase initially and attain maxima of 0.18 and 0.3, respectively, for $[L^6]/[PPh_3]$ = 0.8, concurrent with the formation of the stable ligand-protected Au_8, Au_9, and Au_{10} cluster species. Then, the fractional abundances of chlorinated complexes steadily diminish to nearly 0 at $[L^6]/[PPh_3]$ = 16. The fractional abundance of $[Au_2L^6{}_2]^{2+}$ rapidly increases as L^6 is added until it accounts for nearly all ion signal at $[L^6]/[PPh_3]$ = 16 and correlates with $[Au_8L^6{}_4]^{2+}$ observation in the ESI-MS spectra after reduction. Thus, by selecting the initial metal complex distribution, we can control product formation.

Dynamic light scattering measurements (DLS) of synthesis solutions prepared with the ratios $0.4 \le [L^6]/[PPh_3] \le 16$ show no evidence for any species in solution larger than the detection limit of the instrument (≤1 nm). This result indicates either their absence or that the concentration of clusters above ∼1 nm is below the concentration detection limit for the $[Au_8L^6{}_4]^{2+}$, $[Au_9L^6{}_4Cl]^{2+}$, and $[Au_{10}L^6{}_x]^{2+}$ (x = 4, 5) products. However, reduction of solutions $[L^6]/[PPh_3]$ = 0.25 shows formation of colloids with hydrodynamic diameters larger than 100 nm. In accord with this observation, the UV−vis spectrum (Figure S1, trace A, Supporting Information) shows a faint 520 nm band that may arise from a plasmon resonance of a nanoparticle formed through the reduction of the gold precursor.[17−19] The contrasting behaviors among the syntheses are accounted for by examining the metal complex distributions.

Although $[Au_9L^6{}_4Cl]^{2+}$ is the primary final product formed at $[L^6]/[PPh_3]$ = 1, the succession of species appearing during syntheses suggests similarities of the initial synthetic pathway with other L^n syntheses that do not form Au_9 clusters (Figure 3).[10,16] Initially ($t \le 10$ min), the major products observed in the ESI-MS data are $[Au_8L^6{}_4]^{2+}$ and $[Au_{10}L^6{}_4]^{2+}$ (Figure 3), corresponding to the final ligated Au_8 and Au_{10} clusters reported previously by Bertino et al.;[10] the present UV−vis spectra (Figure S2, Supporting Information) support the previous assignments. At t = 6 days, the distribution of L^6 protected clusters in solution becomes monodisperse $[Au_8L^6{}_4]^{2+}$. Presumably, the nascent larger clusters (e.g., $[Au_{10}L^6{}_x]^{2+}$) have become depleted by ligand etching, leaving almost entirely $[Au_8L^6{}_4]^{2+}$. In turn, by t = 14 days, $[Au_8L^6{}_4]^{2+}$ is largely depleted, and the ESI-MS and UV−vis data indicate that $[Au_9L^6{}_4Cl]^{2+}$ is the principal product (Figure 3) and $[Au_{10}L^6{}_4]^{2+}$ and $[Au_{10}L^6{}_5]^{2+}$ are minor products. Previously, $[Au_8L^n{}_4]^{2+}$ species in solutions for L^n (n = 3, 5) did not persist in solution and behaved as transient species only;[16] the current study shows the $[Au_8L^n{}_4]^{2+}$ as a stable product for specific complex distributions, which may also be observable with other L^n ligands by changing the complex distribution prior to reduction.

DOI: 10.1021/jz1009339 | J. Phys. Chem. Lett. 2010, 1, 2536–2540

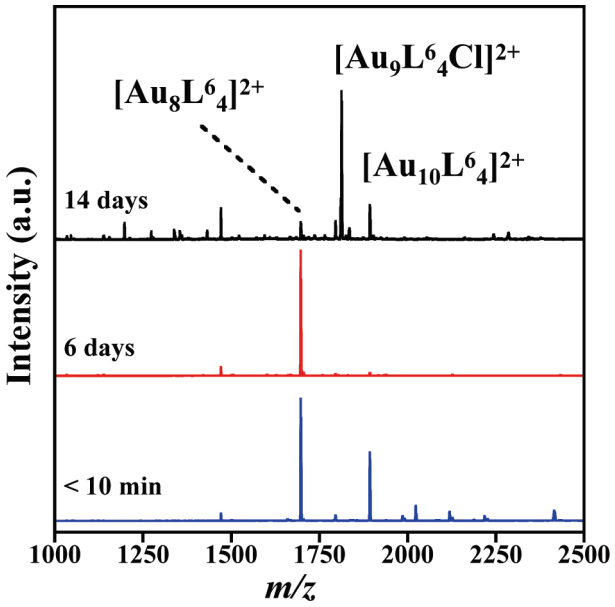

Figure 3. Time-resolved ESI-MS traces for synthesis solutions containing $[L_6]/[PPh_3]$ = 1. The sequence shows that $[Au_9L^6{}_4Cl]^{2+}$ cluster growth is preceded by the formation of monodisperse $[Au_8L^6{}_4]^{2+}$ clusters through degradation of larger clusters.

The observed homogenization of the synthesis products to $[Au_8L^6{}_4]^{2+}$ prior to subsequent formation of $[Au_9L^6{}_4Cl]^{2+}$ and $[Au_{10}L^6{}_x]^{2+}$ is consistent with reaction pathways through $[Au_8L^6{}_4]^{2+}$ (Figure 3). Specifically for this study, nascent formation of the $[Au_{10}L^6{}_x]^{2+}$ in solutions containing $[L^6]/[PPh_3]$ > 0.4 indicates a net addition reaction of neutral gold species

$$[Au_8L^6{}_4]^{2+} + Au^{0''} \rightarrow [Au_9L^6{}_4]^{2+} \quad (1)$$

$$[Au_9L^6{}_4]^{2+} + Au^{0''} \rightarrow [Au_{10}L^6{}_x]^{2+} \quad (2)$$

where protecting ligands on the $Au^{0''}$ are omitted. The protecting ligands of species $Au^{0''}$ in reactions 1 and 2 may include the $Au^0{-}PR_3$ fragment, e.g., $[Au^0{}_2L^6{}_2]$. Schwedtfeger and Boyd have reported relativistic SCF calculations, finding that $[PH_3{-}Au^0{-}Au^0{-}PH_3]$ is stable,[20] and the phenyl groups on PPh_3 or L^6 can further stabilize ligated $Au^0{}_2$ species. Thus, $[Au^0{}_2L^6{}_2]$ and ligated, higher nuclearity Au_x species may comprise the reservoir for $Au^{0''}$. Because these digold species carry no electrical charge, they will be challenging to observe via ESI-MS. Moreover, these will likely be challenging to detect by UV−vis spectroscopy due to spectral overlap with other ligated Au_x clusters. The $[Au_9L^6{}_4]^{2+}$ reaction intermediate is not observed in solution, as is consistent with its 113 valence electron open-shell skeletal configuration that will enhance its reactivity. Although reaction mechanisms can also be developed that contain reduction steps after the addition of one or more Au^I species, this seems unlikely as $NaBH_4$ in methanol reacts to form $NaB(OCH_3)_4$ species with a rate constant of $k = 1.31 \times 10^{-3}$ s^{-1}, which will eliminate the nascent reducing environment within hours,[21] whereas, the formation of larger clusters is active for days.

The formation of $[Au_9L^6{}_4Cl]^{2+}$ indicates that the reaction scheme involves $AuClPPh_3$ or chlorinated tertiary coordination complexes. Since the fractional reaction product $[Au_9L^6{}_4Cl]^{2+}$ diminishes over $0.4 \leq [L^6]/[PPh_3] \leq 2$ (Figure 1) in the region where the equilibrium solution abundances of $[Au_2L^6{}_2Cl]^+$ and $[Au_2L^6{}_3Cl]^+$ are increasing (Figure 2), tertiary complexes do not appear to promote $[Au_9L^6{}_4Cl]^{2+}$ production. The AuCl addition to $[Au_8L^6{}_4]^{2+}$ likely proceeds via

$$[Au_8L^6{}_4]^{2+} + AuClPPh_3 \rightarrow [Au_9L^6{}_4Cl]^{2+} + PPh_3 \quad (3)$$

Because L^6 is a bidentate ligand that is not displaced as $[Au_8L^6{}_4]^{2+}$ reacts with $AuClPPh_3$, reaction 3 differs from that of $[Au_8(PPh_3)_8]^{2+}$,[22] resulting in the attachment of a chloride. Mass spectrometry cannot follow $AuClPPh_3$ directly; however, this species exists in equilibrium with $[Au(PPh_3)_2]^+$.[16,23] The $[Au_9L^6{}_4Cl]^{2+}$ formation is only observed when $Au(PPh_3)_2{}^+$ is detected prior to reduction. The formation of both $[Au_9L^6{}_4Cl]^{2+}$ and $[Au_{10}L^6{}_x]^{2+}$ in molar ratios above 0.4 indicates that reaction 3 occurs preferentially over reactions 1 or 2.

Neither $[Au_9L^6{}_4Cl]^{2+}$ nor $[Au_{10}L^6{}_5]^{2+}$ (nor their PPh_3 analogues) have been reported previously. We account for the stability of these complexes with polyhedral skeletal electron pair (PSEP) theory, which predicts the geometric structures of ligated, closed-shell gold clusters of the form $[Au\{(Au{-}PPh_3)\}_{n_s}]^{z+}$, comprising a central Au surrounded by n_s peripheral $Au{-}PR_3$ fragments.[11−14] To achieve particularly stable structures with closed electron shells, the peripheral fragments are arranged in either spherical or toroidal arrangements, such that the central gold atom has a nine-orbital sp^3d^5 manifold, characterized by a total of $12n_s + 18$ valence electrons, or an eight-orbital sp^2d^5 manifold, characterized by a total of $12n_s + 16$ valence electrons, respectively. The $[Au_9L^6{}_4Cl]^{2+}$ cluster contains 114 valence electrons in a closed-shell, spherical configuration ($n_s = 8 \therefore 114\ e^- = 12n_s + 18$). Analyses of the other clusters also predict stable, closed-shell species, $[Au_8L^6{}_4]^{2+}$ (104 e^-; spherical), $[Au_{10}L^6{}_4]^{2+}$ (124 e^-; toroidal), and $[Au_{10}L^6{}_5]^{2+}$ (126 e^-; spherical). In this work, we have treated $[Au_8L^6{}_4]^{2+}$ and $[Au_9L^6{}_4Cl]^{2+}$ as spherical configurations for which a crystal structure[24] and theoretical description[14] of spherical eight-coordinated Au_8 phosphine cluster are reported in support. However, we note that either structure still represents a stable, closed-shell species if one ligand engages in monodentate complexation. In addition, a crystal structure analogous to $[Au_{10}L^6{}_4]^{2+}$ is reported.[25]

The ligand exchange with L^6 and $AuClPPh_3$ plays a significant role in the formation of the specific cluster sizes by allowing the preservation of the intact precursor material for addition reactions that form the $[Au_9L^6{}_4Cl]^{2+}$ species. By examining the distributions of complexes where only $[Au_8L^6{}_4]^{2+}$ and mostly $[Au_{10}L^6{}_x]^{2+}$ are formed, information about specific complexes can help elucidate information about specific reduction pathways for formation. At the largest $[L^6]/[PPh_3]$, $[Au_8L^6{}_4]^{2+}$ clusters are formed when the metal complex population is nearly all $[Au_2L^6{}_2]^{2+}$, indicating a strong correlation between nonchlorinated complexes and $[Au_8L^6{}_4]^{2+}$ formation. We report the growth of $[Au_9L^6{}_4Cl]^{2+}$ and $[Au_{10}L^6{}_x]^{2+}$ products from the $[Au_8L^6{}_4]^{2+}$ cluster through different addition reactions. At all times, chlorinated clusters are present

DOI: 10.1021/jz1009339 | J. Phys. Chem. Lett. 2010, 1, 2536–2540

when the Au_{10} species are formed, which may suggest that the reduced digold chlorinated complexes are necessary for $[Au_{10}L^6_x]^{2+}$ formation.

The equilibrium between $AuClPPh_3$ and L^6 creates a distinct transition zone centered near $[L^6]/[PPh_3] \approx 3$ that occurs concurrent with the elimination of $[Au(PPh_3)_2]^+$ complexes. In this zone, the initial solution produces $[Au_8L^6_4]^{2+}$ and $[Au_{10}L^6_x]^{2+}$ within days (Figure S3, Supporting Information); however, these complexes subsequently dissolute to gold species of low nuclearity. The instability of these species in synthesis solutions correlates with the relative increase of chlorinated complexes. A possible explanation for the presence of a transition zone may involve the reduction of the less coordinated complexes $[Au(PPh_3)_2]^+$ and $[Au_2L^6_2]^{2+}$ and persistence of chlorinated complexes, $[Au_2L^6_2Cl]^+$ and $[Au_2L^6_3Cl]^+$, lowering the concentration of reduced species in solution.

Classical nucleation theory describes the process of nucleation occurring only during supersaturation conditions with persistence of those species above the critical radius, r^*, at $\Delta G/\Delta r = 0$.[26] It is possible that the specific conditions at $[L^6]/[PPh_3] \approx 3$ form unstable clusters with radii smaller than r^*, which are dissolved back into complexes, as is observed in the current study. The specific roles of varied solution complexes, formed by changing the diphosphine ligand, L^n, and their concentrations will be presented elsewhere, but because the electronic considerations are very similar between L^n (n = 2−6), steric considerations must be a strong contributing factor in the size selectivity.

In conclusion, the role of the metal−ligand complex distribution has been shown to control the product formation of phosphine-protected Au clusters. The synthesis of monodisperse clusters reduces the need for size separation processes. The discovery of the chlorinated $[Au_9L^6_4Cl]^{2+}$ cluster could prove useful in ligand exchange reactions involving phosphine-protected chlorinated clusters.[27,28] The current synthetic method should also prove useful for a broad range of protecting ligands including thiols, amines, and polymeric ligands. Further investigation of the synthetic products from other L^n ligands and the relationship with specific metal−ligand complexes will be presented elsewhere.

EXPERIMENTAL SECTION

We conducted syntheses for the ratios spanning $0 \leq [L^6]/[PPh_3] \leq 18$. Briefly, each synthesis was conducted at 276 K with 10.0 ± 0.1 mg of $AuClPPh_3$ (Sigma Aldrich, 99.9%)[29] dissolved in 15 mL of a 1:1 MeOH/$CHCl_3$ (Sigma Aldrich, HPLC grade; Sigma Aldrich, ACS reagent) mixture within a 20 mL head space vial, and L^6 (Sigma Aldrich, 97%) was added to prepare the desired $[L^6]/[PPh_3]$ ratio. The uncertainty (2σ) associated with the masses of the ligands is ±0.0002 g, correlating to an average 3% uncertainty in the molar ratio with less uncertainty at high molar ratios and as high as ~10% at the lowest L^6 concentrations. $NaBH_4$ (Sigma Aldrich, 98%) reducing agent was added in 4:1 molar excess of Au; the vial was sealed under air, and the solution was stirred by a Teflon-coated magnetic stir bar. Stir bars were not reused. Mass spectrometric measurements were performed with a dual probe electrospray ion source, including an integrated three vacuum stage and ion optics assembly (Analytica of Branford), coupled to a custom-built (by Ardara Technologies) Extrel CMS quadrupole mass spectrometer. Samples were introduced to the ESI source via direct infusion (10 μL/min), and the source was purged with > 1.0 mL of a 1:1 MeOH/$CHCl_3$ solution between each sample. The precision of the fractional ion measurements of each species was ≤10% (2σ) based on five repeated measurements. Source conditions were optimized to maximize ion intensities while minimizing fragmentation. The potential difference between the capillary exit and the skimmer, also termed the in-source collision energy (CE), was usually set to 150 V but could be varied from 20 to 250 V. Sample solutions were further diluted with 1:1 MeOH/$CHCl_3$ to produce relatively stable ion currents. Interpretation of fractional ion intensity measurements presumes that the fractional ion abundance (computed from the ion abundance of each cationic species in a ratio with total ion current) observed by ESI-MS is effectively the same as that in solution.[30,31] Disparate ESI efficiencies between analytes are not expected due to similar functional groups.[16,32]

Optical spectra of solutions were obtained using a Varian Cary II dual beam spectrometer. Dynamic light scattering (DLS) measurements were conducted using a Malvern Zetasizer Nano ZS equipped with a 4 mW, 633 nm (He−Ne) laser. To remove domain-induced scattering of the 1:1 methanol/chloroform solution, samples were diluted with methanol/diethylether before DLS measurements were conducted. The uncertainty of the measurements is reported by the standard deviation of (i) five repeat measurements or (ii) the size distribution change as a function of dilution ratios, whichever is greater. Prior to the addition of the precursor reagents, solvents were prefiltered by a 0.2 μm filter to remove dust. The product from the methanol/$NaBH_4$ reaction was removed with centrifugation. Furthermore, DLS measurements were conducted on solutions containing dissolved ligands, $AuClPPh_3$ alone, $NaBH_4$ alone, and $NaBH_4$ + ligands; these measurements exhibited null results, increasing the acceptance that the DLS distributions derived for reaction solutions correlate to $[Au_xL^6_y]^{z+}$ cluster formation only.

SUPPORTING INFORMATION AVAILABLE

Fractional ion current of solution complexes as a function of $[L_6]/[PPh_3]$ and temporally resolved UV−vis spectra are presented. This material is available free of charge via the Internet at http://pubs.acs.org.

AUTHOR INFORMATION

Corresponding Author:

*To whom correspondence should be addressed. E-mail: jeffrey.hudgens@nist.gov.

Notes

† E-mail: john.pettibone@nist.gov.

ACKNOWLEDGMENT J.M.P. acknowledges the National Academy of Science's National Research Council fellowship.

DOI: 10.1021/jz1009339 | J. Phys. Chem. Lett. 2010, 1, 2536–2540

REFERENCES

(1) Schmid, G.; Pfeil, R.; Boese, R.; Bandermann, F.; Meyer, S.; Calis, G. H. M.; Vandervelden, W. A. $Au_{55}[P(C_6H_5)_3]_{12}Cl_6$. A Gold Cluster of an Exceptional Size. *Chem. Ber.* **1981,** *114*, 3634–3642.

(2) Vandervelden, J. W. A.; Beurskens, P. T.; Bour, J. J.; Bosman, W. P.; Noordik, J. H.; Kolenbrander, M.; Buskes, J. A. K. M. Intermediates in the Formation of Gold Clusters. Preparation and X-Ray-Analysis of $[Au_7(PPh_3)_7]^+$ and Synthesis and Characterization of $[Au_8(PPh_3)_6I]PF_6$. *Inorg. Chem.* **1984,** *23*, 146–151.

(3) Teo, B. K.; Shi, X. B.; Zhang, H. Pure Gold Cluster of 1−9-9−1-9−9-1 Layered Structure: A Novel 39-Metal-Atom Cluster $[(Ph_3P)_{14}Au_{39}Cl_6]Cl_2$ with an Interstitial Gold Atom in a Hexagonal Antiprismatic Cage. *J. Am. Chem. Soc.* **1992,** *114*, 2743–2745.

(4) Hall, K. P.; Mingos, D. M. P. Homonuclear and Heteronuclear Cluster Compounds of Gold. *Prog. Inorg. Chem.* **1984,** *32*, 237–325.

(5) Duan, H. W.; Nie, S. M. Etching Colloidal Gold Nanocrystals with Hyperbranched and Multivalent Polymers: A New Route to Fluorescent and Water-Soluble Atomic Clusters. *J. Am. Chem. Soc.* **2007,** *129*, 2412–2413.

(6) Caragheorgheopol, A.; Chechik, V. Mechanistic Aspects of Ligand Exchange in Au Nanoparticles. *Phys. Chem. Chem. Phys.* **2008,** *10*, 5029–5041.

(7) Schmid, G. The Relevance of Shape and Size of Au_{55} Clusters. *Chem. Soc. Rev.* **2008,** *37*, 1909–1930.

(8) Yanagimoto, Y.; Negishi, Y.; Fujihara, H.; Tsukuda, T. Chiroptical Activity of BINAP-Stabilized Undecagold Clusters. *J. Phys. Chem. B* **2006,** *110*, 11611–11614.

(9) Shichibu, Y.; Konishi, K. HCl-Induced Nuclearity Convergence in Diphosphine-Protected Ultrasmall Gold Clusters: A Novel Synthetic Route to Magic-Number Au_{13} Clusters. *Small* **2010,** *6*, 1216–1220.

(10) Bertino, M. F.; Sun, Z. M.; Zhang, R.; Wang, L. S. Facile Syntheses of Monodisperse Ultrasmall Au Clusters. *J. Phys. Chem. B* **2006,** *110*, 21416–21418.

(11) Mingos, D. M. P. Molecular-Orbital Calculations on Cluster Compounds of Gold. *J. Chem. Soc., Dalton Trans.* **1976,** 1163–1169.

(12) Mingos, D. M. P. Structure and Bonding in Cluster Compounds of Gold. *Polyhedron* **1984,** *3*, 1289–1297.

(13) Mingos, D. M. P. Gold: A Flexible Friend in Cluster Chemistry. *J. Chem. Soc., Dalton Trans.* **1996,** 561–566.

(14) King, R. B. Metal Cluster Topology. 2. Gold Clusters. *Inorg. Chim. Acta* **1986,** *116*, 109–117.

(15) Bardaji, M.; Uznanski, P.; Aniens, C.; Chaudret, B.; Laguna, A. Aurophilic Complexes as Gold Atom Sources in Organic Media. *Chem. Commun.* **2002,** 598–599.

(16) Bergeron, D. E.; Coskuner, O.; Hudgens, J. W.; Gonzalez, C. A. Ligand Exchange Reactions in the Formation of Diphosphine-Protected Gold Clusters. *J. Phys. Chem. C* **2008,** *112*, 12808–12814.

(17) Qian, H. F.; Zhu, M. Z.; Lanni, E.; Zhu, Y.; Bier, M. E.; Jin, R. C. Conversion of Polydisperse Au Nanoparticles into Monodisperse Au_{25} Nanorods and Nanospheres. *J. Phys. Chem. C* **2009,** *113*, 17599–17603.

(18) Alvarez, M. M.; Khoury, J. T.; Schaaff, T. G.; Shafigullin, M. N.; Vezmar, I.; Whetten, R. L. Optical Absorption Spectra of Nanocrystal Gold Molecules. *J. Phys. Chem. B* **1997,** *101*, 3706–3712.

(19) Shem, P. M.; Sardar, R.; Shumaker-Parry, J. S. One-Step Synthesis of Phosphine-Stabilized Gold Nanoparticles Using the Mild Reducing Agent 9-BBN. *Langmuir* **2009,** *25*, 13279–13283.

(20) Schwerdtfeger, P.; Boyd, P. D. W. Role of Phosphine-Ligands in Gold Cluster Chemistry: Relativistic SCF Calculations on Au_2 and $Au_2(PH_3)_2$. *Inorg. Chem.* **1992,** *31*, 327–329.

(21) Davis, R. E.; Gottbrath, J. A. Boron Hydrides 5. Methanolysis of Sodium Borohydride. *J. Am. Chem. Soc.* **1962,** *84*, 895–898.

(22) Vollenbroek, F. A.; Bour, J. J.; Vandervelden, J. W. A. Gold-Phosphine Cluster Compounds: The Reactions of $[Au_9L_8]^{3+}$ (L = PPh_3) with L, SCN^- and Cl^- to $[Au_8L_8]^{2+}$, $[Au_{11}L_8(SCN)_2]^+$ and $[Au_{11}L_8Cl_2]^+$. *Recl. Trav. Chim.* **1980,** *99*, 137–141.

(23) Colton, R.; Harrison, K. L.; Mah, Y. A.; Traeger, J. C. Cationic Phosphine Complexes of Gold(I): An Electrospray Mass-Spectrometric Study. *Inorg. Chim. Acta* **1995,** *231*, 65–71.

(24) Manassero, M.; Naldini, L.; Sansoni, M. New Class of Gold Cluster Compounds: Synthesis and X-Ray Structure of the Octakis(Triphenylphosphinegold) Dializarinsulphonate, $[Au_8(PPh_3)_8](Aliz)_2$. *J. Chem. Soc., Chem. Commun.* **1979,** 385–386.

(25) Briant, C. E.; Hall, K. P.; Wheeler, A. C.; Mingos, D. M. P. Structural Characterization of $[Au_{10}Cl_3(PCy_2Ph)_6](NO_3)$ (Cy = Cyclohexyl) and the Development of a Structural Principle for High Nuclearity Gold Clusters. *J. Chem. Soc., Chem. Commun.* **1984,** 248–250.

(26) Finney, E. E.; Finke, R. G. Nanocluster Nucleation and Growth Kinetic and Mechanistic Studies: A Review Emphasizing Transition-Metal Nanoclusters. *J. Colloid Interface Sci.* **2008,** *317*, 351–374.

(27) Shichibu, Y.; Negishi, Y.; Tsukuda, T.; Teranishi, T. Large-Scale Synthesis of Thiolated Au_{25} Clusters via Ligand Exchange Reactions of Phosphine-Stabilized Au_{11} clusters. *J. Am. Chem. Soc.* **2005,** *127*, 13464–13465.

(28) Brown, L. O.; Hutchison, J. E. Convenient Preparation of Stable, Narrow-Dispersity, Gold Nanocrystals by Ligand Exchange Reactions. *J. Am. Chem. Soc.* **1997,** *119*, 12384–12385.

(29) Certain commercial materials and equipment are identified in this paper in order to adequately specify the experimental procedure. Such identification implies neither recommendation or endorsement by the National Institute of Standards and Technology nor that the material or equipment identified is the best available for the purpose.

(30) Cech, N. B.; Enke, C. G. Practical Implications of Some Recent Studies in Electrospray Ionization Fundamentals. *Mass Spectrom. Rev.* **2001,** *20*, 362–387.

(31) Leito, I.; Herodes, K.; Huopolainen, M.; Virro, K.; Künnapas, A.; Kruve, A.; Tanner, R. Towards the Electrospray Ionization Mass Spectrometry Ionization Efficiency Scale of Organic Compounds. *Rapid Commun. Mass Spectrom.* **2008,** *22*, 379–384.

(32) Di Marco, V. B.; Bombi, G. G. Electrospray Mass Spectrometry (ESI-MS) in the Study of Metal-Ligand Solution Equilibria. *Mass Spectrom. Rev.* **2006,** *25*, 347–379.

DOI: 10.1021/jz1009339 | *J. Phys. Chem. Lett.* **2010,** *1*, 2536–2540